Electrocatalytic oxidation of water by OH^- - and H_2O-capped IrO_x nanoparticles electrophoretically deposited on graphite and basal plane HOPG : effect of the substrate electrode

ChemElectroChem

Chemistry Europe
European Chemical Societies Publishing

Accepted Article

Title: Electrocatalytic Oxidation of Water by OH-- and H2O-Capped IrOx Nanoparticles Electrophoretically Deposited on Graphite and Basal Plane HOPG: Effect of the Substrate Electrode

Authors: Naghmeh Mirbagheri, Rui Campos, and Elena Ferapontova

To be cited as: *ChemElectroChem* 10.1002/celc.202100317

Link to VoR: https://doi.org/10.1002/celc.202100317

WILEY-VCH

WILEY-VCH

ARTICLE

Electrocatalytic Oxidation of Water by OH^-- and H_2O-Capped IrO_x Nanoparticles Electrophoretically Deposited on Graphite and Basal Plane HOPG: Effect of the Substrate Electrode

Naghmehalsadat Mirbagheri[a,b], Rui Campos[a,c], and Elena E. Ferapontova[a]*

[a] Dr. Naghmehalsadat Mirbagheri, Dr.Rui Campos, and Assoc. Prof. Elena E. Ferapontova
Interdisciplinary Nanoscience Center (iNANO), Aarhus University
Gustav Wieds Vej 1590-14, DK-8000 Aarhus C, Denmark
E-mail: elena.ferapontova@inano.au.dk

[b] Dr. Naghmehalsadat Mirbagheri
Department of Microsystems Engineering - IMTEK, University of Freiburg
Georges-Koehler-Allee 103, 79110 Freiburg, Germany

[c] Dr. Rui Campos
AXES research group and NANOlab Center of Excellence
University of Antwerp Groenenborgerlaan 171, 2020,
Antwerpen, Belgium

Supporting information for this article is given via a link at the end of the document.

Abstract: Iridium oxide (IrO_x) is one of the most efficient electrocatalysts for water oxidation reaction (WOR). Here, WOR electrocatalysis by 1.6 nm IrO_x nanoparticles (NPs) electrophoretically deposited onto spectroscopic graphite (Gr) and basal-plane highly ordered pyrolytic graphite (HOPG) was studied as a function of NPs' capping ligands and electrodeposition substrate. On Gr, OH^-- and H_2O-capped NPs exhibited close sub-monolayer surface coverages and specific electrocatalytic activity of 18.9-23.5 mA $nmol^{-1}$ of $Ir^{IV/V}$ sites, at 1 V and pH 7. On HOPG, OH^-–capped NPs produced films with a diminished WOR activity of 5.17±2.40 mA $nmol^{-1}$. Electro-wettability-induced changes impeded electrophoretic deposition of H_2O-capped NPs on HOPG, WOR currents being 25-fold lower than observed for OH^-–capped ones. The electrocatalysis efficiency correlated with hydrophilic properties of the substrate electrodes, affecting morphological and as a result catalytic properties of the formed IrO_x films. These results, important both for studied and related carbon nanomaterials systems, allow fine-tuning of electrocatalysis by a proper choice of the substrate electrode.

Introduction

Replacement of fossil fuels by the alternative clean and renewable energy sources is one of the most challenging problems of the current century. Electrochemical oxidation of water (or the oxygen evolution reaction, OER) may be considered both as a way to provide fuel cells with a clean and sustainable fuel supply and as one of the crucial steps in the process of transforming solar energy into chemically stored energy (O_2 and H_2) within the electrochemical[1-5] and photoelectrochemical/ artificial photosynthesis[6-14] schemes of water splitting. Due to the kinetic impediments and some other factors that reduce the reaction efficiency, direct electrochemical oxidation of water requires an applied potential well beyond the theoretical value (1.23 V versus SHE at 25˚C).[15] That makes the development of highly efficient and stable systems for water oxidation a particularly challenging task.

To overcome the kinetic barrier, a number of robust and efficient catalyst that can function at high turnover rates and low overpotentials have been proposed.[2, 3, 5, 16, 17] Among them, metal oxides such as IrO_2, RuO_2, PtO_2, Co_3O_4, and Mn_2O_3 were shown to efficiently oxidize water.[18-21] Of actual interest is iridium oxide IrO_x, exhibiting the high electrocatalytic activity and performance stability in the OER over a wide pH range (Figure 1).[10, 22-24]

Catalytically active and stable IrO_x electrodes may be produced either by thermal decomposition of the Ir precursor [25] or by the electrochemical treatment of solid iridium electrodes[26, 27] enabling electrooxidation of water at overpotentials, η, ranging between 0.22 and 0.38 V. Generally, IrO_x electrodes prepared by these methods suffer from the low surface area to volume ratio, which unfavourably affects their electrocatalytic properties. Improvement of the catalysis can be achieved with nanomaterials that provide a high surface area to volume ratio, such as IrO_x nanoparticles (NPs). IrO_x NPs with sizes ranging between 1 and 100 nm reduce the η of the water oxidation reaction to 0.20-0.29 V and exhibit a long-term stability and impressive electrocatalytic activity both in acidic and alkaline media. [23, 28-31] Therewith, such factors as experimental conditions for IrO_x NPs synthesis and deposition, NPs capping and the nature of a substrate electrode substantially affect the electrocatalytic activity of IrO_x NPs. Such correlations and dependencies were observed not only for the IrO_x NPs, but also for other electrocatalytic NPs.[32, 33] For example, Zahra et al.[32] showed that the presence of organic phyto-compounds or carbon-containing capping agents used in the synthesis of the PdO–$2Mn_2O_3$ improves the catalytic efficiency of this electrocatalyst toward OER.

Of our particular interest was the effect of capping ligands on the electrocatalytic performance of IrO_x NPs-modified electrodes. Colloidal solutions of IrO_x NPs may be prepared either without or with specific stabilizing (capping) ligands that assist the assembly of IrO_x NPs either immediately onto the electrode or, altogether with other species, in artificial photosynthetic devices.[1, 10, 28, 34-38] Uncapped IrO_x NPs are not so versatile for some of those applications, but they were shown to possess high stability over a wide pH range,[39] whereas capped IrO_x NPs were often reported as tending to aggregate, which resulted in their lower catalytic

activity.[40-42]

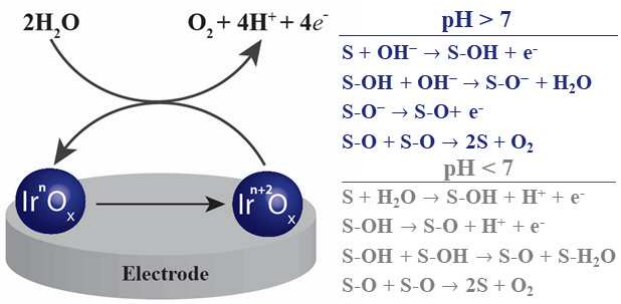

Figure 1. Schematic representation of the electrochemical oxidation of water catalysed by IrO_x NPs.[30, 31, 43-45] (depending on the reaction mechanism *n* can be either 3 [46, 47] or 4 [23]) and the reaction elementary steps in acidic [3, 43, 48] and basic media [15, 30, 44] (S stands for the active site of IrOx at the electrode surface).

In general, the electrocatalytic activity of any IrO_x NPs, both capped and uncapped, depends on the way they prepared and deposited on a substrate electrode. High-surface area IrO_x films exhibiting a high electrocatalytic activity in the OER can be prepared by chemisorption and electrophoretic deposition of IrO_x from its colloidal solutions.[23, 28, 31, 37, 39] Stable 2 nm H_2O-capped $IrO_x \cdot nH_2O$ NPs were produced by treatment of OH^--capped ones with HNO_3; electrophoretically deposited either onto the glassy carbon or spectroscopic graphite (Gr) electrodes, they showed high electrocatalytic activity in the OER within with the broad pH range, from pH 1 to 13.[39] Electro-flocculation of 2 nm OH^--capped IrO_x NPs onto the glassy carbon electrode[23] and of citrate-capped IrO_x NPs onto the ITO electrode[28] also produced highly stable and electrocatalytically active IrO_x NPs electrodes. In another study, Zhao et al.[39] showed that the use of OH^--capped IrO_x NPs for the fabrication of uniform IrO_x thin films on FTO electrodes is accompanied by some difficulties, while uniform films were easily grown on this substrate using the H_2O-capped NPs. Therewith, comparative evaluation of the effects of capping ligands on the electrocatalytic efficiency have not been performed yet, and the prospects of modulation of the electrocatalytic activity of IrO_x NPs by capping are still challenging.

In the present work, electrocatalytic properties of IrO_x NPs electrophoretically deposited onto two types of substrate electrodes, spectroscopic Gr that somehow approaches in its properties the edge-plane highly ordered pyrolytic graphite (HOPG), and basal-plane HOPG, representing a stack of graphene layers and often considered as a first-approximation electrochemical 3D model of graphene,[49] were investigated. These electrode materials have distinctly different surface properties with respect to hydrophilicity/hydrophobicity, surface reactivity[50-54] and surface structural roughness.[55] While the atomically flat surface of HOPG is extremely useful as a substrate for AFM studies,[52, 56, 57] its reactivity is also very attractive for electrochemical applications.[51-54] Cheap and easily renewable spectroscopic Gr, widely used in electroanalysis of small molecules and proteins due to its high-surface area enabling a higher surface coverage with adsorbates,[14, 58-62] has been already used for fabrication of IrO_x nanocomposite electrodes.[31] These electrodes demonstrated the hitherto highest electrocatalytic current densities, of 43 mA cm^{-2} at 1 V and pH 7, in OER.[31] In the present work, IrO_x NPs were synthesized with either OH^- or H_2O as capping ligands (further referred to as OH^-- and H_2O-capped NPs, respectively). NPs were electrophoretically deposited onto the electrodes and interrogated in the reaction of electrochemical oxidation of water at different pHs. We aimed at finding correlations between the electrocatalytic reactivity of NPs and their capping lingand properties as well as with the nature of the substrate electrode.

Results and Discussion

Characterization of OH^-- and H_2O-capped IrO_x NPs by UV-Vis spectroscopy

During the IrO_x NPs synthesis, K_2IrCl_6 was hydrolysed in basic medium to $[Ir(OH)_6]^{2-}$. The absorbance spectrum of the basic solution (Figure 2, line 1) showed a peak at around 313 nm corresponding to the monomeric $[Ir(OH)_6]^{2-}$ complex. At sufficiently high concentrations, the $[Ir(OH)_6]^{2-}$ monomers were partially polymerized and formed IrO_x NPs capped with hydroxide anions (OH^--capped IrO_x NPs). The OH^--capped IrO_x NPs exhibited a broad visible band around 585 nm, which is characteristic of Ir^{IV} oxide (Figure 2, line 1).

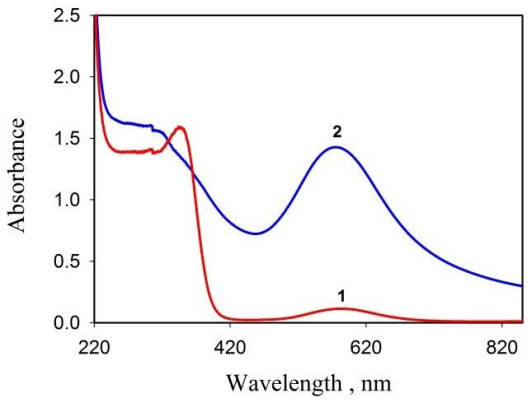

Figure 2. Representative UV-Vis spectra of the synthesized (1) OH^-- and (2) H_2O-capped IrO_x NPs colloids after overnight storage.

Acidification of the basic solution was accompanied by protonation of OH^--capped IrO_x NPs and their condensation with the remained $[Ir(OH)_6]^{2-}$ species. That resulted in the formation of H_2O-capped IrO_x NPs and the disappearance of the peak at 313 nm (Figure 2, line 2).[30, 63] H_2O-capped IrO_x NPs also exhibited the Ir^{IV} oxide peak at around 575 nm, in accordance with earlier reports.[30, 39] Based on the reported extinction coefficients (630±50, and 3370±10 M^{-1} cm^{-1} for IrO_x NPs at 574 nm and $[Ir(OH)_6]^{2-}$ at 313 nm, respectively),[39] the estimated concentrations of IrO_x NPs in basic and acidic media were 0.18 mM and 2.3 mM, respectively, indicating a lower yield of IrO_x NPs in basic solutions.

Characterization of IrO_x NPs by TEM. Zeta-potential determination

The size distribution of the synthesized IrO_x NPs is presented in Figure 3. As can be seen, OH^--and H_2O-capped IrO_x NPs

possess almost the same size, with diameters of 1.69±0.24 and 1.6±0.19 nm, corresponding to 80 and 66 Ir sites per OH^-- and H_2O-capped NPs, respectively. [64]

At neutral pH, zeta potentials of the synthesized OH^-- and H_2O-capped IrO_x NPs were -27.4 mV and -13.7 mV, respectively. Thus, both bear a net negative charge. The more negative ξ-potential of the OH^--capped IrO_x NPs may provide their higher stability and then the less tendency for aggregation compared to H_2O-capped ones. In acidic solutions, a partial protonation of OH^--capped IrO_x NPs may lead to the formation of H_2O-capped NPs, with a less negative ξ-potential, which in its turn should trigger the NPs aggregation. Zeta potential values obtained for OH^--capped IrO_x NPs at neutral pH are consistent with ca. -35 mV shown for IrO_2 powders at pH 6-10.[65] However, the ξ-potential of -13.7 mV estimated here for H_2O-capped IrO_x NPs is more consistent with the value observed in the same work at pH 4.[65] We may suggest that water/capping ligand properties strongly depend on the IrO_x NPs size (though, direct correlations with IrO_2 powders are not possible, the IrO_2 size was not reported)[65] and are quite different from those expected for bulk materials. Such suggestion is consistent with the weak dependence of the IrO_2 powder ξ-potentials on the solution ionic strength. [65] Thus, H_2O-capping of 1.6 nm IrO_x NPs appears to be stronger than expected for larger size particles and does not exchange for OH^--capping ligand at neutral pH.

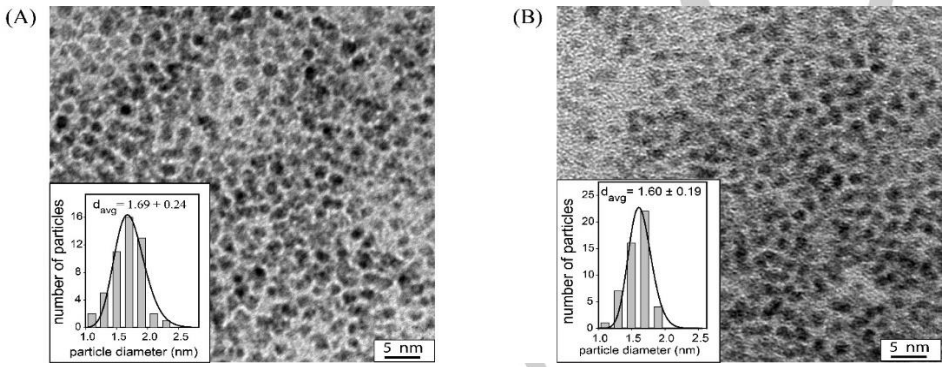

Figure 3. TEM images of the (A) OH^-- and (B) H_2O-capped IrO_x NPs (scale bars are 5 nm).

Electrocatalysis of water oxidation by IrO_x NPs: effect of a capping ligand and the substrate electrode.

Gr electrodes were electrophoretically modified either with OH^--capped or H_2O-capped IrO_x NPs. The electrocatalytic activity of H_2O-capped IrO_x NPs-modified Gr electrodes in water oxidation was measured first at pH 1.5 and then consecutively at higher pHs, whereas the experiments with OH^--capped IrO_x NPs-modified Gr electrodes were first performed at pH 13 and then in solutions of lower pHs. The overall electrocatalysis started at potentials essentially lower than the reaction at bare Gr electrodes (ESI, Figures S1 and S2, dotted lines). Both OH^-- and H_2O-capped IrO_x NPs-modified Gr electrodes showed a quite similar electrocatalytic activity in water oxidation (Figure 4), with the oxidation current densities, at 1V and pH 7, of 37.9±2.9 and 34.7±2.2 mA cm^{-2} and the reaction overpotentials of 0.19 and 0.20 V (the electrocatalysis onset at 0.628 and 0.618 V), respectively. That was in agreement with the results reported previously for H_2O-capped IrO_x-modified Gr.[31]

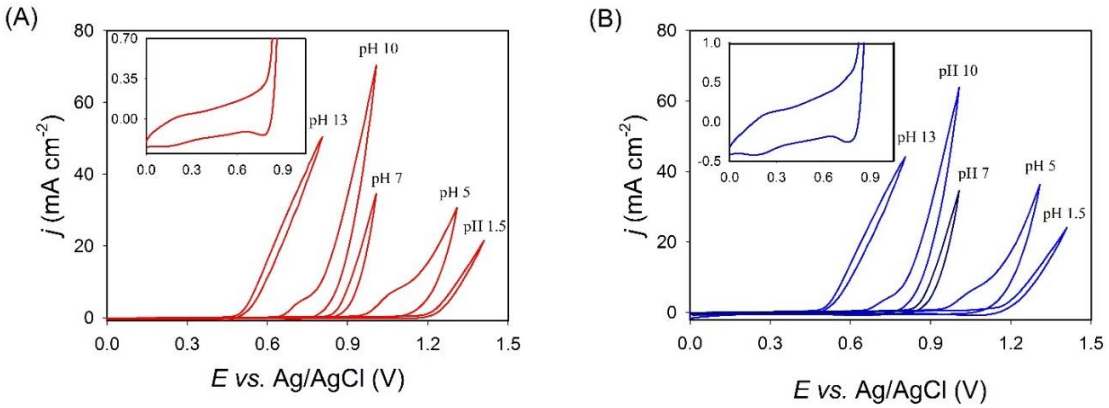

Figure 4. Representative CVs of the electrocatalytic oxidation of water recorded at different pHs with (A) OH^--capped and (B) H_2O-capped IrO_x NPs-modified Gr electrodes. Inset: zoomed potential window corresponding to the non-catalytic IrO_x NPs redox chemistry at pH 7.The axis titles in the inset are the same as in the main figure. Potential scan rate: 20 mV s^{-1}.

Therewith, two redox processes could be followed at potentials lower than OER potentials, consistent with the Ir^{III}/Ir^{IV} and Ir^{IV}/Ir^{V} redox transformations[31] (Figure 4, insets). Due to the essential capacitive currents, those peaks were ill-defined within the full-scale CVs. However, after the polynomial background correction they become pronounced enough both for the peak potential determination and for the peak integration (Figure S3, ESI). For the OH^--capped IrO_x-modified Gr electrodes, the formal potential for the Ir^{III}/Ir^{IV} and Ir^{IV}/Ir^{V} redox couples ($E^{0'}$) at pH 7 was +0.15 V and +0.55 V, correspondingly. For the H_2O-capped IrO_x-modified Gr electrodes, the $E^{0'}$ was, respectively, +0.21 V and +0.54 V. The overall electrochemistry of both NPs-modified electrodes agreed well with previous reports on IrO_x-NPs electrophoretically deposited onto different substrates. [23, 28, 30, 31] The Ir^{III}/Ir^{IV} surface coverage, $\Gamma_{Ir(III/IV)}$, for the OH^-- and H_2O-capped IrO_x on Gr (Table 1) corresponded to ca. 39×10^{12} and 42×10^{12} NPs cm^{-2} of a geometric surface area, respectively. The total area occupied e.g. by 39×10^{12} OH^--capped IrO_x NPs was then 1.1 cm^2per cm^2 of the geometric electrode surface, calculated in assumption of 1.69×1.69 nm^2 occupied by one NP. It was consistent with a sub-monolayer coverage if the electrode surface roughness was taken into account (the Gr roughness factor is at least 5). [55, 66] These $\Gamma_{Ir(III/IV)}$ are lower than reported in our previous work,[31] however the specific electrocatalytic activity of these electrodes was still high, reaching the electrocatalytic current densities reported for higher surface coverages of NPs. The most important, no distinctive preferential interactions of either OH^-- or H_2O-capped IrO_x NPs with the Gr substrate could be followed: both types of NPs were electrophoretically deposited onto Gr in a consistently similar manner providing similar electrocatalysis patterns as well.

Table 1. Electrocatalytic activity of the OH^-- and H_2O-capped IrO_x NPs electrodeposited onto Gr and HOPG in the water oxidation reaction at pH 7

Modified electrode	$\Gamma_{(Ir^{III}/Ir^{IV})}$ nmol cm^{-2}	$\Gamma_{(Ir^{IV}/Ir^{V})}$ nmol cm^{-2}	i mA cm^{-2} [c]	$i/\Gamma_{(Ir^{IV}/Ir^{V})}$ mA $nmol^{-1}$
OH^--capped IrO_x-modified Gr	5.17±1.22	1.61±0.78	37.9±2.9	23.5±7.92
H_2O-capped IrO_x-modified Gr	4.56±2.67	1.83±0.56	34.7±2.2	18.93±2.97
OH^--capped IrO_x-modified HOPG	3.84±2.23	1.76±0.84	9.1±2.2	5.17±2.40
H_2O-capped IrO_x-modified HOPG	n.d.	n.d.	0.36±0.02	-

$\Gamma_{(Ir^{III}/Ir^{IV})}$ and $\Gamma_{(Ir^{III}/Ir^{IV})}$ are surface coverage values estimated by integration of the Ir^{III}/Ir^{IV} and Ir^{IV}/Ir^{V} peaks, respectively; i is current density at 1 V; $i/\Gamma_{(Ir^{IV}/Ir^{V})}$ is the current density normalized to the value of $\Gamma_{(Ir^{IV}/Ir^{V})}$, suggested to be directly involved in electrocatalysis [11, 23]. n.d. = not detectable.

In contrast to Gr, electrophoretic deposition of OH^-- and H_2O-capped IrO_x NPs onto basal plane HOPG showed a different pattern and revealed clear distinctions between these two substrates.

First, though the electrocatalytic performance of the OH^--capped IrO_x NPs deposited on the HOPG electrodes followed the same pattern as that for Gr, a four-to-three-fold lower electrocatalytic current densities in OER were observed (Figure 5). This only partially may be attributed to a smaller true surface area of the HOPG electrodes. Second, electrooxidation of water by H_2O-capped IrO_x NPs deposited onto HOPG from acidic solutions was essentially less efficient (e.g., at pH 13, the catalytic current densities were two orders of magnitude lower). For OH^--capped IrO_x NPs, a thick IrO_x film visible with a naked eye was formed on the HOPG surface exposed to the working solution. In the case H_2O-capped IrO_x NPs, no film formation was detected, and AFM surface studies of NPs were not successful, either due to the small surface concentration or/and weak adhesion of H_2O-capped IrO_x NPs to the HOPG surface. In the course of electrocatalytic studies in solutions of different pH (changing from pH 1.5 to 13, Figure 5B), the activity of H_2O-capped IrO_x NPs-modified HOPG reduced substantially. That was not observed with OH^--capped NPs (Figure 5A).

The stability of the H_2O-capped IrO_x NPs deposited on Gr and HOPG electrodes was further compared by recording CVs in solutions of different pH, starting from pH 10 to 1.5 (ESI, Figure S4A, solid lines) and *vice versa*, from pH 1.5 to 10 (Figure S4A, dashed lines). For the H_2O-capped IrO_x-modified Gr electrodes, forward and backward CVs recorded at each pH were quite similar; the same pattern was shown for OH-capped IrOx NPs deposited on Gr and HOPG. However, the H_2O-capped IrO_x-modified HOPG electrodes were not stable, and current densities differed when CVs were run first in acidic and then in basic solutions as compared to first running in basic and then in acidic solutions (ESI, Figure S4B). It is worth to mention that the electrocatalytic activity of the modified HOPG electrodes was anyway essentially improved compared to the bare HOPG: the onset potential of the water oxidation reaction at the HOPG electrode was 199 mV reduced (0.619 V at pH 7) after electrode modification with IrO_x NPs (ESI, Figures S5-S7).

Non-catalytic CVs recorded with the OH^--capped IrO_x-modified HOPG showed two couples of peaks corresponding to the IrO_x transformation at +0.23 V (Ir^{III}/Ir^{IV}) and +0.42 V (Ir^{IV}/Ir^{V}). A general waveform was quite different from that observed on Gr, and the Ir^{IV}/Ir^{V} peak potentials were 120-130 mV less positive than on Gr (Figure 5A, inset). With the H_2O-capped IrO_x-modified HOPG, these redox transformations were undetectable (Figure 5B, inset). For OH^--capped IrO_x NP electroflocculated on HOPG, the Ir^{III}/Ir^{IV} surface coverage (Table 1) correlated with 29×10^{12} NP cm^{-2}. It is comparable with that observed on Gr, but provided less efficient electrocatalysis of water oxidation, due to the possible NP aggregation/cluster formation on the surface of HOPG. While shown on Gr 39×10^{12} and 42×10^{12} NP cm^{-2}, when referred to the true surface area of the Gr electrodes (the roughness factor of 5) result in a less than 20% of the monolayer coverage, OH^--capped IrO_x NPs occupy ca. 0.89 cm^2 of the HOPG surface. That, taking into account the 0.135 cm^2 surface of HOPG, exceed the monolayer surface density. Then analysis of the efficiency of electrocatalytic oxidation of water (current densities in Figures 4 and 5 and data in Table 1) suggests that the denser package of NPs on HOPG inhibits the electrocatalytic activity of NPs due to either NP-neighbouring effects or NPs aggregation.

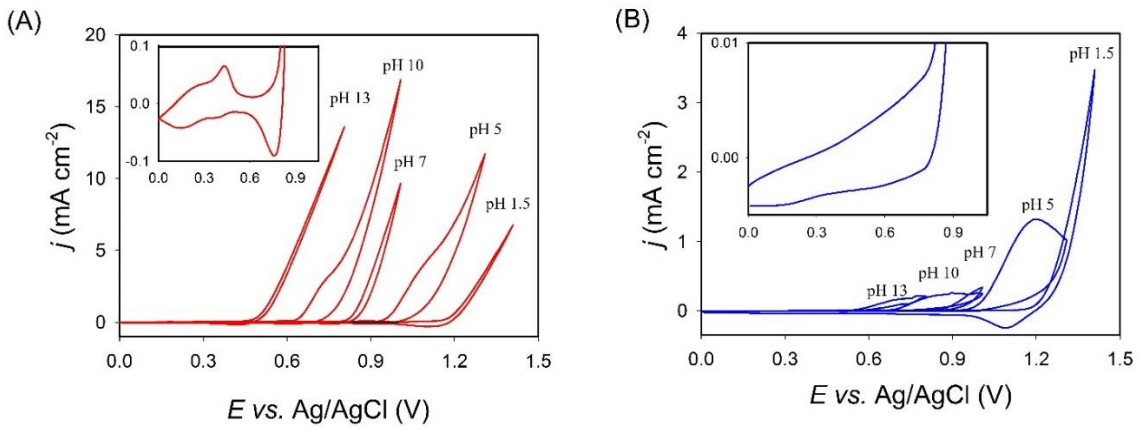

Figure 5. Representative CVs of the electrocatalytic oxidation of water recorded at different pHs with (A) OH^--capped and (B) H_2O-capped IrO_x NPs-modified HOPG electrodes. Inset: zoomed potential window corresponding to the IrO_x NPs redox peaks at pH 7. The axis titles in the inset are the same as in the main figure. Potential scan rate is 20 mV s^{-1}.

Water oxidation mechanism at IrO_x-modified Gr and HOPG electrodes

The mechanism of water oxidation in aqueous acidic solutions (pH 1.5) electrocatalysed by OH^-- or H_2O-capped IrO_x NPs deposited on Gr and HOPG electrodes was assessed by the analysis of the Tafel plots constructed from the electrocatalytic CV forward scans recorded at 20 mV s^{-1}; this scan rate is slow enough for a proper kinetic analysis of the process not limited by diffusion of the discharging species (the H_2O concentration is 55.5 M). Under those conditions, only one region of linearity was observed for the OH^--capped IrO_x-modified Gr electrode (Figure 6, line 1), H_2O-capped IrO_x-modified Gr electrode (Figure 6, line 2), and H_2O-capped IrO_x-modified HOPG electrodes (Figure 6, line 4) with the slopes of 98, 134, and 70 mV dec^{-1}, respectively.

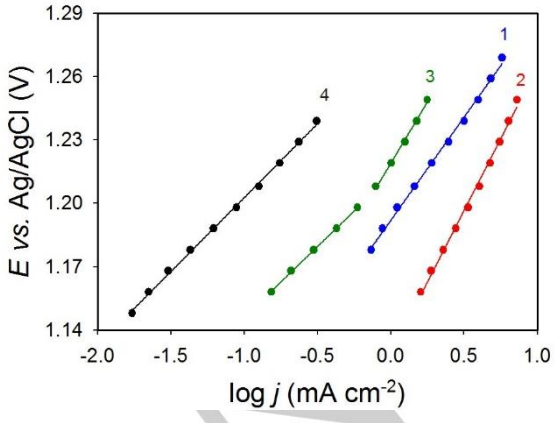

Figure 6. Representative Tafel plots for the OER on (1) the OH^--capped IrO_x-modified Gr, (2) the H_2O-capped IrO_x-modified Gr, (3) the OH^--capped IrO_x-modified HOPG and (4) the H_2O-capped IrO_x-modified HOPG electrode, pH 1.5. The Tafel slopes are (1) 98 ± 2 mV dec^{-1}, (2) 134 ± 3 mV dec^{-1}, (3) 67 ± 1 and 116 ± 4 mV dec^{-1}, and (4) 70±1 mV dec^{-1}.

In the case of the OH^--capped IrO_x-modified HOPG, two linear regions with the Tafel slopes of 67 mV dec^{-1}, at lower potentials, and 116 mV dec^{-1}, at higher potentials, were observed (Figure 6, line 3), which may be assigned to two different rate determining steps in water oxidation reaction in acidic solutions:[43, 67]

$$S + H_2O \rightarrow S\text{-}OH^* + H^+ + e^- \quad (1)$$
$$S\text{-}OH^* \rightarrow S\text{-}OH \quad (2)$$
$$S\text{-}OH \rightarrow S\text{-}O + H^+ + e^- \quad (3)$$
$$S\text{-}O + S\text{-}O \rightarrow 2S + O_2 \quad (4)$$

where S stands for the active sites of the IrO_x catalyst and S-OH* is the intermediate that precedes the formation of S-OH. The Tafel slope close to 60 mV dec^{-1} (at lower potentials) indicates that the chemical step (2) is the rate determining step if the coverage of the S-OH groups is high enough,[43, 45] whereas the Tafel slope close to 120 mV dec^{-1} correlates with the electrochemical step (1).[48, 68] Therefore, for the OH^--capped IrO_x-modified HOPG electrode either (1) or (2) can determine the reaction rate, depending on the applied potential. The Tafel slopes most consistent with 120 mV dec^{-1} (98 ± 2 and 134 ± 3 mV dec^{-1}) observed for the IrO_x-modified Gr electrodes (Figure 6, lines 1 and 2) suggest that the rate determining step for these electrodes is (1), whereas in the case of H_2O-capped IrO_x-modified HOPG electrode (Figure 6, line 4) the slope of 70±1 mV dec^{-1} suggests (2) as the rate determining step of the OER.

Surface reactivity of the Gr and HOPG electrodes

The specific electrocatalytic activity of the IrO_x-modified Gr and HOPG electrodes, i.e. referred to the number of electrocatalytic sites, was evaluated and compared. For that, the electrocatalytic current densities of water oxidation were referred to the surface coverage of the electrochemically active IrO_x estimated by integration of the IrO_x redox peaks wherever it was possible (Table 1).

As can be seen from Table 1, the surface coverage of OH^-- and H_2O-capped NPs deposited on Gr electrodes and thus the state of NPs on these electrodes was very similar (Table 1). This

explains very close water oxidation overpotentials and the electrocatalysis efficiency. For basal plane HOPG, very different surface coverages were obtained for OH^--capped and H_2O-capped NPs, with the former approaching that on Gr and with the latter being undetectable. That accounts for the higher electrocatalytic activity of OH^--capped IrO_x NPs on HOPG, though their specific electrocatalytic activity dropped approximately four-fold compared to that of OH^--capped IrO_x NPs on spectroscopic Gr.

The optical microscope and SEM examination of the HOPG surface morphology showed that the HOPG surface exposed to the suspensions of OH^--capped IrO_x NPs was mostly covered with IrO_x NPs and their aggregates (Figure 7A,B), also seen with a naked eye. In contrast, only a few H_2O-capped NPs or their possible aggregates were detected on HOPG (Figure 7C), consistent with a negligible IrO_x surface coverage evaluated from CVs (Figure S7). In the case of OH^--capped IrO_x-modified Gr, it was impossible to detect neither individual nor aggregated NPs on the Gr surface due to its roughness that did not allow the nm-magnification requested (Figure S8). This was in agreement with the presence of rather dispersed than aggregated OH^--capped IrO_x NPs exhibiting the highest electrocatalytic activity (Table 1).

Strikingly different patterns of the electrophoretic deposition of H_2O- and OH^--capped IrO_x NPs on basal plane HOPG could be connected with a different reactivity of the substrate electrode in acidic and basic media. In particular, electrochemically induced changes in surface wettability[69, 70] might affect both electroflocculation and aggregation of NPs on the HOPG surface. Compared to Gr, HOPG demonstrated better wettability both by acidic and basic solutions (Figure 8A), with a contact angle approaching 64° reported for freshly cleaved HOPG.[71] However, under 1.3 V polarization applied, for the H_2SO_4 solution drop, pH 1.5, the contact angle decreased from 63.3°±2.8° to 35.3°±0.5° demonstrating a medium-specific increasing hydrophilicity of the surface (Figure 8B and mediafiles enclosed in ESI visualizing electrowetting of the HOPG surface in H_2SO_4 and NaOH media). Therewith, no electro-wettability effects could be followed when a NaOH drop, pH 13, was placed on the HOPG surface, and the contact angle of 56° remained virtually the same at open circuit potential (56.1°±7.7°) and under 1.3 V applied (55.9°±6.6°).

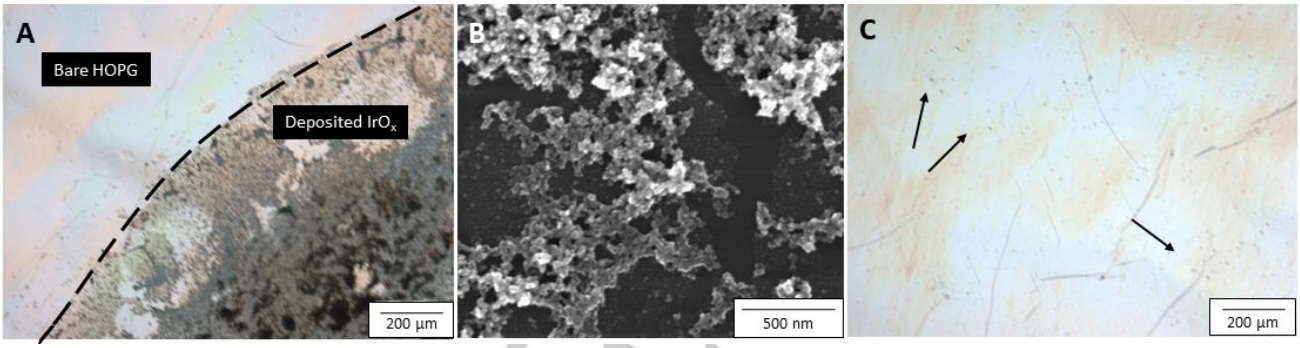

Figure 7. (A, C) Optical images of (A) OH^--capped and (C) H_2O-capped IrO_x-modified HOPG, and (B) a SEM image of OH^--capped IrO_x-modified HOPG. In (A) the dashed line represents the border between the unmodified HOPG area and the region exposed to electrophoretic deposition of NPs. In (C) the arrows point to some areas where NPs were electrophoretically deposited.

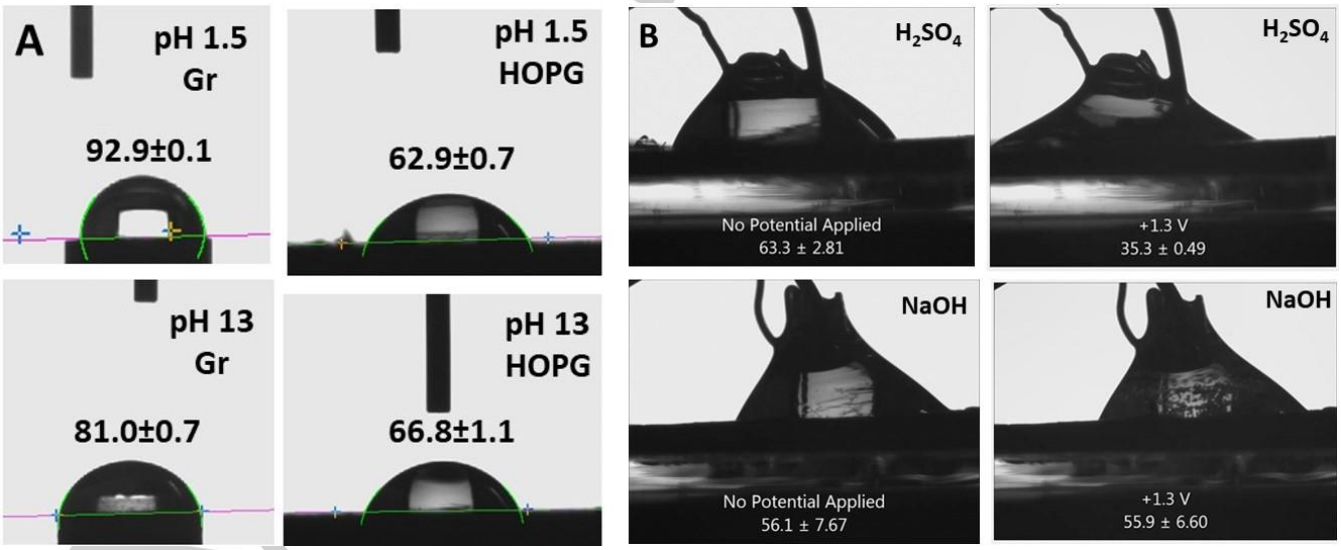

Figure 8. Microscopic images of a 5 µL drop of aqueous solutions of H_2SO_4, pH 1.5, and NaOH, pH 13; on (A) bare Gr and basal plane HOPG; and (B) on basal plane HOPG with no potential applied and under 1.3 V polarization; Pt wire and Ag/AgCl wire were used as counter pseudo-reference electrodes. The corresponding contact angles values are indicated in each image.

Consistent with previous reports, electrowetting of the HOPG surface by the H_2SO_4 solution drop is primarily connected with the intercalation of SO_4^{2-} ions into HOPG. [70] As therein extensively shown, at oxidative potentials perchlorate, nitrate and sulphate anions can intercalate into the stacked graphene layers of HOPG through the surface step edges that are negatively charged versus the underlying basal surface bearing a neutral charge. The overall process results in the boosted electrowetting of HOPG via the insertion of the oxygen containing ions.[70] A more recent report discusses the observed electrowetting in pseudicapacitor terms: the anion intercalation causes an increase in the HOPG capacitance, which drives the enhancement of electrowetting at the voltage >1 V, resulting in the increased spreading of the electrolyte drop on the surface of HOPG. [72]

Thus, the enhanced electrowettability of basal plane HOPG in acidic solutions, from which H_2O-capped IrO_x NPs were electrophoretically deposited, affected the surface reactivity and adsorption properties of HOPG and led to different patterns of the OH- and H_2O-capped NPs electrophoretic deposition. In basic solutions, the surface properties of HOPG unchanged under the 1.3 V polarization and were close to those of spectroscopic Gr. That enabled the NPs electroflocculation onto HOPG that followed the pattern similar to Gr and resulted in the comparable surface coverages with NPs. Along with that, the flatter morphology of the HOPG surface and, supposedly, a higher hydrophilicity resulted in the formation of the IrO_x film composed of the aggregated IrO_x NPs. In contrast to that, the electrowetting of the HOPG surface (in acidic solutions from which the H_2O-capped IrO_x NPs were electrophoretically deposited) did not facilitate deposition of IrO_x NPs sufficient for electrocatalysis and formation of a stable IrO_x NPs layer. Keeping in mind that ion intercalation plays important role in HOPG exfoliation and production of graphene flakes,[70] we can also guess that 1.3 V electrophoretic deposition of H_2O-capped IrO_x NPs in the presence of anionic intercalators, such as SO_4^{2-} or and NO_3^-, could affect the integrity of the stacked graphene layers and made the NPs deposition and surface adhesion less efficient.

Thus, the analysis of the effect of capping ligands on the electrocatalytic performance of NPs-modified electrodes is apparently complicated by the nature of the conductive substrate support, which was already discussed to strongly contribute not only to the NP Fermi level but also to the surface dispersion and aggregation of NPs on the electrode surface.[38] The lower wettability (i.e., higher hydrophobicity) of spectroscopic Gr in combination with its highly micro-structured surface composed of graphitic flakes[54, 55] enable electrophoretic deposition of IrO_x NPs minimally aggregated and with a maximal specific electrocatalytic activity. Independently of the time of deposition, no solid IrO_x NPs films could be formed on the Gr electrodes.[31] That also results from the adsorption-desorption equilibria established during two processes proceeding during the electrophoretic deposition: the deposition itself and the simultaneous rigours oxygen gas evolution electrocatalysed by NPs being deposited. We speculate that on Gr each newly deposited NP occupies a new surface space, avoiding the aggregation. Electrophoretic deposition of OH^--capped IrO_x NPs on more wettable (more hydrophilic) and atomically flat basal plane HOPG is then more compatible with hydrophilic IrO_x NPs. The electrophoretic deposition under those conditions results in the formation of a densely packed IrO_x film composed of aggregated NPs, with each next NP interacting with the already deposited one.

Interestingly, a comparison of IrO_x surface coverages on Gr (Table 1) with the surface coverages reported for more hydrophilic (the contact angle 60°)[73] glassy carbon, with its from 10 to 70 nmol $Ir^{IV/V}$ deposited per cm^2 reported,[23, 30] shows that the electrophoretic deposition of IrO_x NPs on a more hydrophobic Gr results in a lower $Ir^{IV/V}$ surface coverage indeed. However, this lower $\Gamma_{IrIV/IrV}$ on Gr provides specific electrocatalytic current densities (Table 1) higher than IrO_x NPs film-modified glassy carbon (from 0.3 to 1.9 mA $nmol^{-1}$ at 1 V and pH 7).[23, 39] The results obtained with the glassy carbon electrodes correlate with a higher extent of NPs aggregation, similarly to shown with HOPG in basic solutions. Thus, we suggest that more hydrophilic substrates may promote NPs surface aggregation during the electrophoretic deposition, while less hydrophilic surfaces enable the electrophoretic deposition of individual non-aggregated NPs with a higher reactivity.

Conclusion

1.6 nm IrO_x NPs with either OH^- or H_2O capping ligands were synthesized and electrophoretically deposited at 1.3 V from basic and acidic solutions, correspondingly, onto the surface of spectroscopic Gr and basal plane HOPG electrodes. Their electrocatalytic activity was interrogated. Both the deposition media and the nature of the deposition substrate influenced the morphological and electrocatalytic properties of the deposited IrO_x NPs. The electrophoretic deposition of OH^- and H_2O-capped IrO_x NP onto the less hydrophilic Gr surface resulted in the nanocomposite electrodes with electrocatalytic properties superior to those of the IrO_x-modified HOPG. The "hydrophilic compatibility" between NPs and HOPG lead to the deposition of IrO_x NPs films composed of NPs aggregates with a lower reactivity, while less hydrophilic spectroscopic Gr produced a highly reactive sub-monolayer of NPs. In acidic solutions, electrowettability effects resulted in a low-efficient electrophoretic deposition of individual (not aggregated) IrO_x NP on basal plane HOPG, whose electrocatalytic activity was negligible due to their very low surface coverage. The obtained results contribute to further understanding on how deposition and electrocatalytic properties of NPs can be tuned by a proper choice of the substrate electrodes and may be relevant for some other carbon nanocomposite such as graphene- and carbon nanotubes-based.

Experimental Section

Materials. All experiments were performed at 22±1°C if not stated otherwise; solutions were prepared with 18.2 MΩ de-ionized Milli-Q water (Millipore, Bedford, MA, USA). K_2IrCl_6 (99.99%), NaOH (98%), H_2SO_4 (95-97%), H_3PO_4 (85%) were purchased from Sigma-Aldrich. HNO_3 (68%) was from Riedel-deHaen. Buffer solutions were prepared from 1 M H_3PO_4 and pH was adjusted to 5, 7, and 10 using concentrated NaOH. Solutions with pH 1.5 and pH 13 (un-buffered) were prepared from the corresponding H_2SO_4 and NaOH solutions, respectively.

Synthesis of $IrO_x.nH_2O$ NPs

$IrO_x.nH_2O$ NPs were produced by the protocol established by Mallouk et al. [39] Briefly, a 2 mM solution of OH^--capped IrO_x NPs was prepared by dissolving an appropriate amount of K_2IrCl_6 in water. The pH of the solution was adjusted to pH 13 by adding 4 M NaOH. The resulting solution was

heated up to 90°C for 20 min under continuous stirring and then cooled down in an ice bath, turning a pale purple colour. [74] The 2 mM solution of H_2O-capped-IrO_x NPs was prepared from the cooled, basic solution of OH^--capped IrO_x NPs by rapid addition of 4 M HNO_3 until pH 1 was achieved (under stirring). [39] Solution stirring was continued for 80 min until the solution colour changed to deep blue. The resulting solutions of OH^--capped and H_2O-capped IrO_x NPs were aged for at least one day and used for modification of the electrodes, being kept in the refrigerator between the modification procedures.

Characterization of NPs

Spectrophotometric characterization. Spectrophotometric properties and concentration of IrO_x NPs in acidic (pH 1) and basic (pH 13) solutions were determined by monitoring the increase in absorbance within 200-1000 nm range using a Shimadzu UV-Vis-NIR spectrophotometer UV-3600 (Shimadzu Corporation, Japan).

Transmission Electron Microscopy (TEM). TEM imaging of the OH^--capped and H_2O-capped-IrO_x NPs used for electrode modifications was done by a 200 keV TEM (CM20, Philips) and a CCD camera. Prior to the TEM imagining, the studied suspensions were diluted, and a 2 µl drop of the examined suspension was placed onto the TEM grid (200 mesh copper grid with formvar/carbon support film, Ted Pella Inc.) and dried by a vacuum pump.

Dynamic Light Scattering (DLS). DLS measurements were performed in solutions containing 1 mg ml^{-1} IrO_x NPs and 10 mM NaCl. ξ-potentials was measured with a Zetasizer Nano (Malvern Instruments Ltd, UK) with a backscatter angle of 173°. Zeta-potentials were estimated by processing data within the Smoluchowski model. [75]

Microscopy. The optical images were recorded with a commercial optical microscope Olympus BX51, Japan (a 5X objective lens with numerical aperture of 0.15). The surface of the IrO_x-modified Gr and HOPG electrodes was characterized using a scanning electron microscope (SEM, FEI Nova NanoSEM 600) equipped with an energy dispersive spectrometer.

Electrode modification and electrochemical measurements

Gr disk electrodes (∅ 0.3 cm rods of solid spectroscopic graphite, type RW001, Werk Ringsdorff, Germany, fitted in Teflon holders) were used as working electrodes. Graphite rods were cut and polished on fine emery paper and further on Kimwipes® wipers (Kimberly-Clark Professional). The HOPG electrode was produced by exfoliating basal-plane oriented HOPG (grades ZYA and ZYB, Advanced Ceramics Inc., Cleveland, OH, and NT-MDT) using an adhesive band and placing it in a home-made Teflon holder, leaving a 0.415 cm in diameter surface of HOPG exposed to solution. IrO_x NPs were electrophoretically deposited onto the electrode surface from either OH^-- or H_2O-capped 2 mM IrO_x NPs solutions (either basic or acidic, correspondingly) by applying a deposition potential of 1.3 V for 10 min, according to the optimised protocol previously established for IrO_x NPs deposition on Gr. [31] The same modified electrode was used in the water oxidation reaction over the pH1.5 - 13 range. All over the work we used the "aged" solutions of $IrO_x{\cdot}nH_2O$ NPs, shown to be stable for at least one month while kept in a fridge.

Cyclic voltammetry (CV) was performed in a standard three-electrode electrochemical cell with an Ag/AgCl (3 M KCl) and a Pt wire as the reference electrode and auxiliary electrodes, respectively. The electrodes were connected to an AUTOLAB PGSTAT 300 (Eco Chemie, the Netherlands) equipped with a GPES 4.9 software. The reproducibility of the data, at each pH, was verified by measurements with at least three equivalently prepared electrodes. Voltammetric data analysis such as the redox peak potential determination, peak background polynomial correction and integration was performed using the GPES 4.9 software; peak deconvolution and integration was also performed by the graphical software Origin 8. The overpotentials of the OER were estimated as a difference between the thermodynamic potential of the OER and the experimentally observed onset potentials for the OER obtained from Tafel plots.

Acknowledgements

The work was supported by the Aarhus University starting grant to EF. We greatly appreciate Dr. Yuya Hayashi's assistance with the DLS measurements and Jacques Chevallier – with TEM measurements.

Keywords: Electrocatalysis • water oxidation reaction • iridium oxide nanoparticles • graphite • basal plane highly ordered pyrolytic graphite (HOPG)

[1] A. A. Gambardella, N. S. Bjorge, V. K. Alspaugh, R. W. Murray *J. Phys. Chem. C*. **2011**, *115*, 21659-21665.
[2] C. C. L. McCrory, S. Jung, I. M. Ferrer, S. M. Chatman, J. C. Peters, T. F. Jaramillo *J. Am. Chem. Soc*. **2015**, *137*, 4347-4357.
[3] S. Chen, S. S. Thind, A. Chen *Electrochem. Commun.* **2016**, *63*, 10-17.
[4] M. Fang, G. Dong, R. Wei, J. C. Ho *Adv. Energ. Mater*. **2017**, *7*, 1700559.
[5] M. E. G. Lyons, R. L. Doyle, M. P. Browne, I. J. Godwin, A. A. S. Rovetta *Curr. Opin. Electrochem.* **2017**, *1*, 40-45.
[6] N. S. Lewis *Nature*. **2001**, *414*, 589-590.
[7] V. Balzani, A. Credi, M. Venturi *ChemSusChem*. **2008**, *1*, 26-58.
[8] D. Gust, T. A. Moore, A. L. Moore *Acc. Chem. Res.* **2009**, *42*, 1890-1898.
[9] R. Abe *J. Photochem. Photobiol., C*. **2010**, *11*, 179-209.
[10] F. A. Frame, T. K. Townsend, R. L. Chamousis, E. M. Sabio, T. Dittrich, N. D. Browning, F. E. Osterloh *J. Am. Chem. Soc.*. **2011**, *133*, 7264-7267.
[11] N. Mirbagheri, D. Wang, C. Peng, J. Wang, Q. Huang, C. Fan, E. E. Ferapontova *ACS Catalysis*. **2014**, *4*, 2006-2015.
[12] T. Grewe, M. Meggouh, H. Tüysüz *Chem. Asian J*. **2016**, *11*, 22-42.
[13] L. Zhang, I. Álvarez-Martos, A. Vakurov, E. E. Ferapontova *Sustain. Energ. Fuels*. **2017**, *1*, 842-850.
[14] P. Lopes, K. Koschorreck, J. Nedergaard Pedersen, A. Ferapontov, S. Lörcher, J. Skov Pedersen, V. B. Urlacher, E. E. Ferapontova *ChemElectroChem*. **2019**, *6*, 2043-2049.
[15] H. Dau, C. Limberg, T. Reier, M. Risch, S. Roggan, P. Strasser *ChemCatChem*. **2010**, *2*, 724-761.
[16] B. Limburg, E. Bouwman, S. Bonnet *Coord. Chem. Rev*. **2012**, *256*, 1451-1467.
[17] D. G. H. Hetterscheid, J. N. H. Reek *Angew. Chem., Int. Ed.* **2012**, *51*, 9740-9747.
[18] G. Beni, L. M. Schiavone, J. L. Shay, W. C. Dautremont-smith, B. S. Schneider *Nature*. **1979**, *282*, 281-283.
[19] A. Harriman, I. J. Pickering, J. M. Thomas, P. A. Christensen *J. Chem. Soc., Faraday Trans. 1*. **1988**, *84*, 2795-2806.
[20] F. Jiao, H. Frei *Angew. Chem., Int. Ed.* **2009**, *48*, 1841-1844.
[21] F. Jiao, H. Frei *Energy Environ. Sci.* **2010**, *3*, 1018-1027.
[22] L. Badia-Bou, E. Mas-Marza, P. Rodenas, E. M. Barea, F. Fabregat-Santiago, S. Gimenez, E. Peris, J. Bisquert *J. Phys. Chem. C*. **2013**, *117*, 3826-3833.
[23] T. Nakagawa, C. A. Beasley, R. W. Murray *J. Phys. Chem. C*. **2009**, *113*, 12958-12961.
[24] K. E. Michaux, R. W. Murray *Langmuir*. **2013**, *29*, 12254-12258.
[25] S. Fierro, T. Nagel, H. Baltruschat, C. Comninellis *Electrochem. Commun.* **2007**, *9*, 1969-1974.
[26] C. S. Johnson, J. T. Hupp *J. Electroanal. Chem.* **1993**, *345*, 351-362.
[27] T. Reier, M. Oezaslan, P. Strasser *ACS Catalysis* **2012**, *2*, 1765-1772.
[28] T. Kuwabara, E. Tomita, S. Sakita, D. Hasegawa, K. Sone, M. Yagi *J. Phys. Chem. C*. **2008**, *112*, 3774-3779.

[29] M. C. Chuang, J. A. A. Ho *RSC Adv.* **2012**, *2*, 4092-4096.
[30] Y. X. Zhao, N. M. Vargas-Barbosa, E. A. Hernandez-Pagan, T. E. Mallouk *Small*. **2011**, *7*, 2087-2093.
[31] N. Mirbagheri, J. Chevallier, J. Kibsgaard, F. Besenbacher, E. E. Ferapontova *ChemPhysChem*. **2014**, *15* 2844-2850.
[32] T. Zahra, K. S. Ahmad, A. G. Thomas, C. Zequine, R. K. Gupta, M. A. Malik, M. Sohail *RSC Adv*. **2020**, *10*, 29961-29974.
[33] J. Creus, S. Drouet, S. Suriñach, P. Lecante, V. Collière, R. Poteau, K. Philippot, J. García-Antón, X. Sala *ACS Catalysis*. **2018**, *8*, 11094-11102.
[34] W. J. Youngblood, S. H. A. Lee, K. Maeda, T. E. Mallouk *Acc. Chem. Res.* **2009**, *42*, 1966-1973.
[35] S. H. A. Lee, Y. X. Zhao, E. A. Hernandez-Pagan, L. Blasdel, W. J. Youngblood, T. E. Mallouk *Faraday Discuss*. **2012**, *155*, 165-176.
[36] N. D. Morris, T. E. Mallouk *J. Am. Chem. Soc*. **2002**, *124*, 11114-11121.
[37] M. Yagi, E. Tomita, T. Kuwabara *J. Electroanal. Chem.* **2005**, *579*, 83-88.
[38] P. Peljo, M. D. Scanlon, A. J. Olaya, L. Rivier, E. Smirnov, H. H. Girault *J. Phys. Chem. Lett*. **2017**, *8*, 3564-3575.
[39] Y. X. Zhao, E. A. Hernandez-Pagan, N. M. Vargas-Barbosa, J. L. Dysart, T. E. Mallouk *J. Phys. Chem. Lett.* **2011**, *2*, 402-406.
[40] M. Hara, T. E. Mallouk *Chem. Commun.* **2000**, 1903-1904.
[41] M. Hara, J. T. Lean, T. E. Mallouk *Chem. Mater.* **2001**, *13*, 4668-4675.
[42] P. G. Hoertz, Y. I. Kim, W. J. Youngblood, T. E. Mallouk *J. Phys. Chem. B*. **2007**, *111*, 6845-6856.
[43] J. M. Hu, J. Q. Zhang, C. N. Cao *Int. J. Hydr. Energ*. **2004**, *29*, 791-797.
[44] V. I. Birss, A. Damjanovic *J. Electrochem. Soc.* **1987**, *134*, 113-117.
[45] K. Endo, Y. Katayama, T. Miura, T. Kishi *J. Appl. Electrochem.* **2002**, *32*, 173-178.
[46] M. Busch, E. Ahlberg, I. Panas *J. Phys. Chem. C*. **2013**, *117*, 288-292.
[47] P. Steegstra, M. Busch, I. Panas, E. Ahlberg *J. Phys. Chem. C*. **2013**, *117*, 20975-20981.
[48] E. Slavcheva, I. Radev, S. Bliznakov, G. Topalov, P. Andreev, E. Budevski *Electrochim. Acta*. **2007**, *52*, 3889-3894.
[49] D. A. C. Brownson, D. K. Kampouris, C. E. Banks *Chem. Soc. Rev*. **2012**, *41*, 6944-6976.
[50] D. K. Kampouris, C. E. Banks *Chem. Commun*. **2010**, *46*, 8986-8988.
[51] A. N. Patel, M. G. Collignon, M. A. O'Connell, W. O. Y. Hung, K. McKelvey, J. V. Macpherson, P. R. Unwin *J. Am. Chem. Soc.* **2012**, *134*, 20117-20130.
[52] A. G. Güell, A. S. Cuharuc, Y.-R. Kim, G. Zhang, S.-y. Tan, N. Ebejer, P. R. Unwin *ACS Nano*. **2015**, *9*, 3558-3571.
[53] I. Álvarez-Martos, E. E. Ferapontova *Electrochem. Commun.* **2018**, *89*, 48-51.
[54] I. Álvarez-Martos, E. E. Ferapontova *Electroanalysis*. **2018**, *30*, 1082-1090.
[55] V. Castaing, I. Álvarez-Martos, E. E. Ferapontova *Electrochim. Acta*. **2016**, *197*, 263-272.
[56] P. Lopes, M. Xu, M. Zhang, T. Zhou, Y. Yang, C. Wang, E. E. Ferapontova *Nanoscale* **2014**, *6*, 7853-7857.
[57] R. Campos, S. Zhang, J. M. Majikes, L. C. C. Ferraz, T. H. LaBean, M. D. Dong, E. E. Ferapontova *Chem. Commun.* **2015**, *51*, 14111-14114.
[58] F. B. Emre, P. Lopes, E. E. Ferapontova *Electroanalysis*. **2014**, *26*, 1354-1361.
[59] E. Fernandez, J. T. Larsson, K. J. McLean, A. W. Munro, L. Gorton, C. von Wachenfeldt, E. E. Ferapontova *Electrochim. Acta*. **2013**, *110* 86-93.
[60] S. Lörcher, P. Lopes, A. Kartashov, E. E. Ferapontova *ChemPhysChem*. **2013**, *14*, 2112-2124.
[61] M. Sosna, Bonamore A., Gorton L., Boffi A., E. E. Ferapontova *Biosens. Bioelectron.* **2013**, *42*, 219-224.
[62] M. Sosna, N. Leiva-Eriksson, L. Bülow, E. E. Ferapontova *ChemElectroChem*. **2020**, *7*, 2114-2122.
[63] G. Van Loon, J. A. Page *Can. J. Chem.* **1966**, *44*, 515-520.
[64] M. A. El Khakani, M. Chaker, E. Gat *Appl. Phys. Lett.* **1996**, *69*, 2027-2029.
[65] A. Vitins, O. A. Petrii, B. B. Damaskin, Y. A. Ermakov, A. Grzejdziak, E. L. Kolomnikova, S. A. Sukhishvili, A. A. Yaroslavov *Russ. J. Electrochem.* **1992**, *28*, 404-413.
[66] H. Jaegfeldt, T. Kuwana, G. Johansson *J. Am. Chem.Soc.*. **1983**, *105*, 1805-1814.
[67] L. A. Da Silva, V. A. Alves, M. A. P. Da Silva, S. Trasatti, J. F. C. Boodts *Can. J. Chem.* **1997**, *75*, 1483-1493.
[68] G. N. Martelli, R. Ornelas, G. Faita *Electrochim. Acta*. **1994**, *39*, 1551-1558.
[69] D. J. Lomax, P. Kant, A. T. Williams, H. V. Patten, Y. Zou, A. Juel, R. A. W. Dryfe *Soft Matter*. **2016**, *12*, 8798-8804.
[70] G. Zhang, M. Walker, P. R. Unwin *Langmuir*. **2016**, *32*, 7476-7484.
[71] A. Kozbial, F. Zhou, Z. Li, H. Liu, L. Li *Acc. Chem. Res.* **2016**, *49*, 2765-2773.
[72] B. Tang, W. Shao, J. Groenewold, H. Li, Y. Feng, X. Xu, L. Shui, J. Barman, G. Zhou *Phys.Chem. Chem. Phys.* **2019**, *21*, 26284-26291.
[73] K. Calfumán, J. Honores, M. Isaacs, D. Quezada, J. Valdebenito, M. Urzúa *Electroanalysis*. **2019**, *31*, 671-677.
[74] L. Wöhler, W. Witzmann *Z. Anorg. Chem.* **1908**, *57*, 323-352.
[75] R. J. Hunter, Zeta potential in colloid science: principles and applications, Academic Press, London; New York, **1981**.

Entry for the Table of Contents

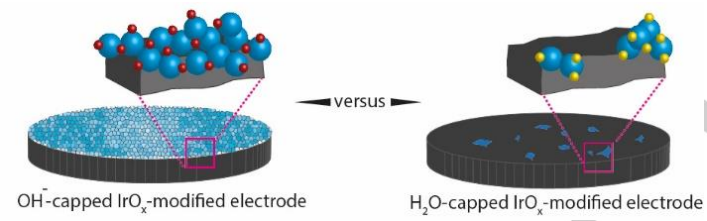

IrO_x NPs are one of the most efficient electrocatalysts for water oxidation. We show that the efficiency of electrocatalytic oxidation of water by differently capped IrO_x NPs electrophoretically deposited onto Gr and basal plane HOPG electrodes from basic and acidic solutions can be correlated with the surface morphology and hydrophilicity/hydrophobicity of the substrate electrodes.